Earthquakes and Structures, *Vol. 13, No. 3 (2017) 309-322*
DOI: http://dx.doi.org/10.12989/eas.2017.13.3.309

A simplified evaluation method of skeleton curve for RC frame with URM infill

Kiwoong Jin[1a] and Ho Choi*[2]

[1]*Department of Architectural and Building Science, Tohoku University, Sendai, Japan*
[2]*Institution of Industrial Science, The University of Tokyo, Tokyo, Japan*

(Received March 2, 2016, Revised November 8, 2017, Accepted November 15, 2017)

Abstract. In this paper, a simplified evaluation method of the skeleton curve for reinforced concrete (RC) frame with unreinforced masonry (URM) infill is proposed in a practical form, based on the previous studies. The backbone curve for RC boundary frame was modeled by a tri-linear envelope with cracking and yielding points. On the other hand, that of URM infill was modeled by representative characteristic points of cracking, maximum, and residual strength; also, the interaction effect between RC boundary frame and the infill was taken into account. The overall force-displacement envelopes by the sum of RC boundary frame and URM infill, where the backbone curves of the infill from other studies were also considered, were then compared with the previous experimental results. The simplified estimation results from this study were found to almost approximate the overall experimental results with conservative evaluations, and they showed much better agreement than the cases employing the infill envelopes from other studies.

Keywords: RC frame; URM infill; diagonal strut mechanism; backbone curve; ASCE41-06

1. Introduction

Serious earthquake damage, resulting in catastrophic building collapse, on reinforced concrete (RC) frames with unreinforced masonry (URM) infills is commonly found in parts of Asia, Europe, and Latin America. The URM infills have been considered secondary elements in structural design stage, and building engineers have paid less attention to their effects on the structural performance, although URM infills interact with boundary RC frames. Therefore, the seismic performance evaluation of URM infills in RC frames is very crucial to mitigate their earthquake damage.

The study on seismic behavior of URM infills started more than 50 years ago. Holmes (1961) suggested URM infill in boundary frames as a pin-jointed diagonal bracing system, and equivalent diagonal strut width was proposed as 0.3 times the diagonal length of the infill, but the boundary frame consisted of steel material. Stafford Smith and Carter (1969) also assumed that URM infill behaves as equivalent diagonal strut, and the equivalent strut width was proposed based on the concept of contact length between boundary columns and infills. Herein, the contact length was based on the relative stiffness between boundary columns and infills, which was derived from elastic beam theory (Hetenyi 1946). Unreinforced concrete or mortar infill were, however, mainly employed for the infill material, and the boundary frame was also steel material. Mainstone (1971) used brick masonry for URM infills, and an empirical equation for equivalent diagonal strut width was proposed. In the study (Mainstone 1971), the equivalent diagonal strut width proposed by Stafford Smith and Carter was modified based on the experiment results, but it had a tendency to underestimate the equivalent strut width (Al-Chaar 2002). On the other hand, Paulay and Priestley (1992) proposed the equivalent strut width as 25% of the diagonal length of URM infill, where the infills were also replaced for a diagonally braced system. FEMA 306 (1998), FEMA 356 (2005), and ASCE41-06 (2006) adopted the equivalent diagonal strut width proposed by Mainstone (1971), although it showed lower evaluation results than others (Al-Chaar 2002). Despite the work conducted on this topic, the change of diagonal strut mechanism and its lateral strength along with the lateral drift angle were rarely considered. Therefore, to evaluate the lateral strength of infills with different levels of lateral deformation, in-plane cyclic loading tests of one-bay, small-scaled RC specimens with URM infills were carried out by authors (Jin *et al.* 2016). In this experiment, a distinctive measurement scheme using 3-axis strain gauges, attached on all URM units, was employed to investigate how to and how much the infill contributes to the overall frame. Also, the diagonal strut mechanism and lateral load carrying capacity of URM infills were successfully explained, based on the experimental data using principal compressive strains of the infills and the strain-stress relationship of URM wallettes.

In this study, as a next step, an appropriate skeleton curve for the RC frame with URM infill, which can be used for simplified performance-based design, is developed. Concerning the backbone curves of the infills, Bertoldi *et al.* (1993) proposed the skeleton curve, based on the relative stiffness between boundary columns and infills. The curve has three characteristic points to represent the force-

*Corresponding author, Research Associate
E-mail: choiho@iis.u-tokyo.ac.jp
[a]Assistant Professor

ISSN: 2092-7614 (Print), 2092-7622 (Online)

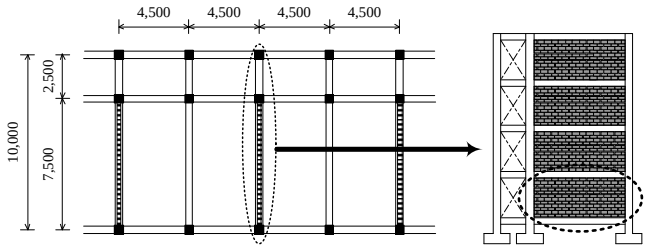

Fig. 1 Standard design of Korean 4-story school buildings in the 1980's (unit: mm)

displacement relationship, where the equivalent strut model is considered. Panagiotakos and Fardis (1996) also proposed the force-displacement curve of the infill, based on the equivalent strut model. For modeling of the curve, however, some additional factors such as shear modulus and tensile strength of the infill are required, which needs extra material tests. Moreover, the softening branch after peak strength and residual infill strength are somewhat unclear. ASCE41-06 (2006) and FEMA356 (2005) have proposed the envelop curve for URM infill confined by surrounding RC frame. However, they do not consider the diagonal strut mechanism of the infill, which is one of the main failure mode, and the residual strength of the infill is not available in the provisions. Stavridis and Shing (2012) proposed a simplified modeling method of masonry-infilled RC frames subjected to seismic loads, based on FE analysis. However, they treated the infill and surrounding RC frame as a single structural system, and the lateral stiffness and strength of overall structure were discussed, based on the shear-beam concept (Fiorato *et al*. 1970). That is, the shear and flexural behaviors of a cantilever composite beam, consisting of RC columns and URM infill, were considered, although obvious damage from diagonal strut was found in the infill. Also, the sliding shear failure mode of the infill was mainly taken into account, where the specific values of some crucial factors (cohesion strength of mortar joints, friction coefficient and vertical load applied on the infill) to calculate the sliding shear strength are not clearly indicated. The most accurate approach using numerical and computational nonlinear micro-models was also carried out by some researchers (Shing and Stavridis 2014, Fiore *et al*. 2012, Caliò and Pantò 2014), but they are usually very complicated and require high computational effort.

As mentioned above, the research concerning practical prediction methods of the envelope curve for this type of structure, which can be used for the simplified performance-based design, seems still insufficient, and some of them require complicated analysis. Therefore, in this paper, a simplified evaluation method of the skeleton curve for RC frames with URM infills was proposed, based on the previous experimental results and studies. The total force-displacement envelopes consisting of RC boundary frames and URM infills were then compared with the previous test results and literatures. It should be also noted that the opening effect of the infill on its seismic capacity (Onur Ozturkoglu *et al*. (2017) is an important issue, but the scope of this study concerned with URM infills without openings.

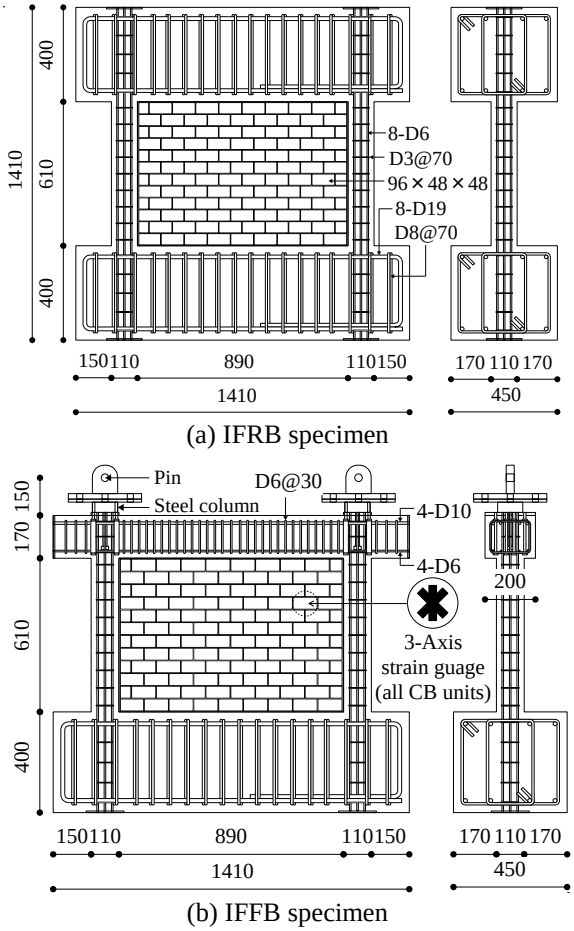

Fig. 2 Details of specimens (unit: mm)

2. Experimental investigation of lateral strength for URM-infilled RC frame

As mentioned earlier, the lateral load carried by RC boundary frame and URM infill was experimentally investigated in the previous study by authors. The experimental outline and the lateral load of URM-infilled RC frame are briefly described, as follows. Detailed experiment results and procedures are provided by Jin *et al*. (2016).

2.1 Experimental outline

In the previous study (Jin *et al*. 2016), the test specimens were designed according to the standard design of Korean 4-story school buildings in the 1980's shown in Fig. 1 (KMCT 2002). From this prototype building, two types of 1/4-scaled specimens, infilled frame with rigid beam (IFRB) and infilled frame with flexible beam (IFFB), having an axial load level of their first story were designed, as shown in Fig. 2, and their in-plane cyclic loading tests were carried out. Herein, the URM infill consisted of unreinforced concrete block units. Three-axis strain gauges were then attached on all URM units (total 114 units) to estimate the detailed strain states of URM infill, which was the key point of the measurement plan, as shown in Fig. 3, and their strain data were employed to evaluate the

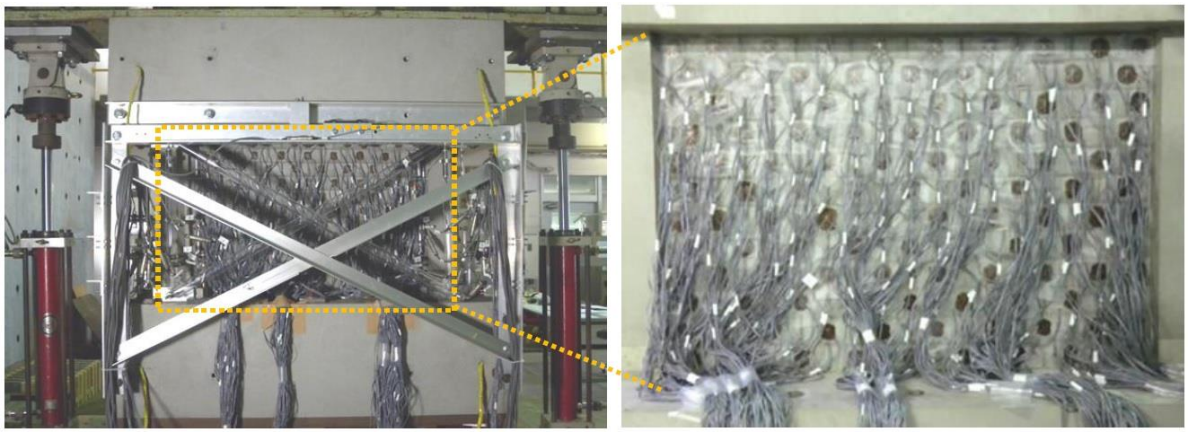

Fig. 3 Key point of the measurement plan (three-axis strain gauges on all URM units)

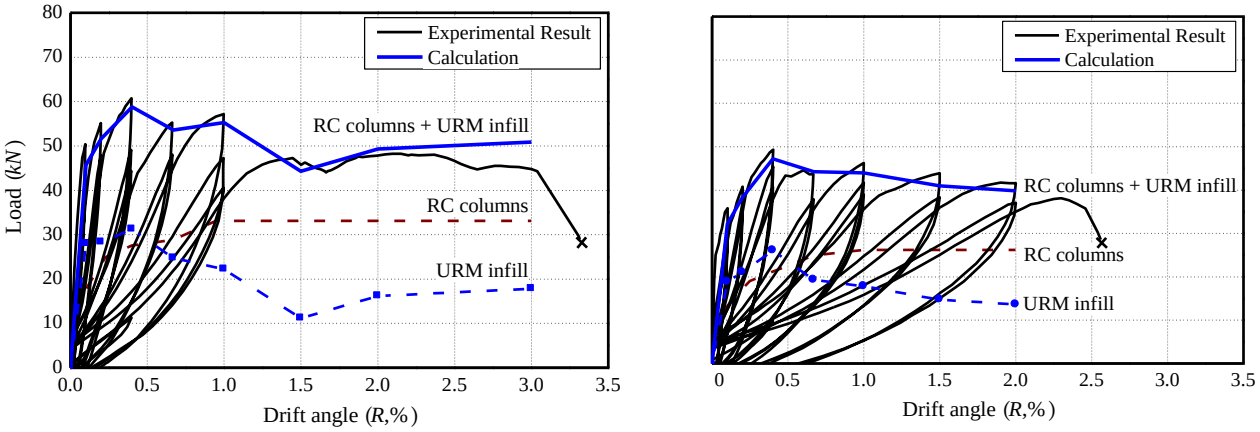

(a) IFRB specimen (b) IFFB specimen

Fig. 4 Lateral strength evaluation of IFRB and IFFB specimens based on experimental data

equivalent diagonal strut width and shear capacity of the infill.

2.2 Lateral load carried by RC boundary frame and URM infill

The lateral load carried by RC columns and URM infills in IFRB and IFFB specimens were evaluated by using experimental data in the previous study (Jin *et al*. 2016), and they were compared to the test results, as shown in Fig. 4. In the figure, the lateral load carried by RC columns was calculated from their curvature and assumed moment distribution. On the other hand, that of URM infill was estimated based on the principal compressive strain acting on the diagonal strut and the strain-stress relationship of URM wallettes. As shown in Fig. 4, the sum of both contribution by RC boundary frames and URM infills well agreed with the overall response recorded in both specimens. In the next chapter, a simplified modeling method to practically estimate the skeleton curve of URM-infilled RC frame will be further discussed, based on the previous experimental results and studies.

3. A simplified skeleton curve evaluation of URM-infilled RC frame

3.1 A Simplified skeleton curve for RC boundary frame

In the simplified evaluation, the skeleton curve for RC boundary frame is modeled by tri-linear, as shown in Fig. 5, which is usually employed for RC bare frame. Herein, the cracking moments (M_c, M_b) and initial stiffness K_c of the column are calculated according to theoretical Eqs. (1) through (3) (AIJ 2010). The secant stiffness $\alpha_y \cdot K_c$ of the column is estimated according to Eq. (4), which was derived from a number of experimental results over 200 specimens to evaluate the yielding deformation of RC members (Sugano 1970) and was adopted by AIJ (2010).

The ultimate bending moments of the column (M_{cu}) and beam (M_{bu}) are calculated based on the simplified Eqs. (5) and (6) (AIJ 2010). Otherwise, M_{cu} and M_{bu} can be also evaluated from the plane-section assumption, where the ultimate strain ε_{cu} at the concrete compression fiber is set to be 0.003 with an equivalent rectangular stress block coefficient from ACI (2011). It should be noted that all these equations and methods are generally applied to predict and reproduce the lateral load-deformation curve of RC bare frame in Japan, as shown in Fig. 6, where the test results of bare frame specimens, preceded this study, are exemplified.

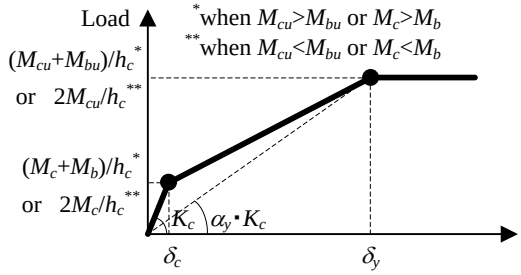

Fig. 5 Tri-linear envelope for boundary frame (one column)

$$M_c = 0.56\sqrt{\sigma_B} Z_e + ND/6 \tag{1}$$

$$M_b = 0.56\sqrt{\sigma_B} Z_e \tag{2}$$

$$K_c = \left(\frac{h_c^3}{12EI_c} \cdot \frac{12\rho + 4}{12\rho + 1} + \kappa h / GA \right)^{-1}, \quad \rho = \frac{\sum EI_b / l_b}{\sum EI_c / h_c} \tag{3}$$

$$\alpha_y = (0.043 + 1.64np_t + 0.43\alpha / D + 0.33\eta_0) \cdot (d/D)^2 \tag{4}$$

$$M_{cu} = 0.8a_t\sigma_y D + 0.5ND \cdot \left(1 - \frac{N}{bD\sigma_c}\right) \tag{5}$$

$$M_{bu} = 0.9a_t\sigma_y d \tag{6}$$

where M_c is the cracking moment of column, M_b is the cracking moment of beam, σ_B is the compressive strength of concrete, Z_e is the section modulus, N is the column axial force, D is the column cross-section height, h_c is the column height, E is the Young's modulus of concrete, I_b is the moment of inertia of beam, l_b is the beam length, I_c is the moment of inertia of column, k is the section shape factor (1.5), G is the shear modulus of concrete, A is the column section area, n is the Young's modulus ratio of reinforcement and concrete, p_t is the longitudinal reinforcement ratio of column, α/D is the shear span ratio of column, η_0 is the axial force ratio of column, d is the effective cross-section height, a_t is the tensile reinforcement area, σ_y is the tensile reinforcement strength, and D is the column depth.

For an actual case, the effective height and seismic behavior of RC columns with URM infill could be somewhat different with those in bare frames due to the infill. From the previous experiment (Jin *et al*. 2016), such effective height change was also observed especially in the tensile columns, behaving as a short column, due to URM infill. However, the effective height and behavior of the tensile column were found to be gradually closer to those in bare frames, as the damage of UMR infill progressed; moreover, the lateral strength and stiffness of RC boundary frames with the infills would be conservative estimates from the aforementioned equations. Therefore, in this study, those equations are employed for simplified and conservative modeling of the envelope curve for RC boundary frame with URM infill.

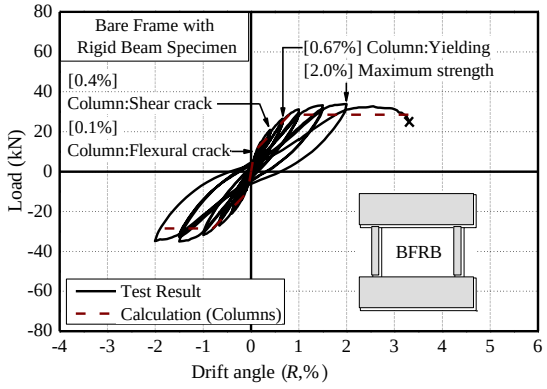

(a) BFRB specimen

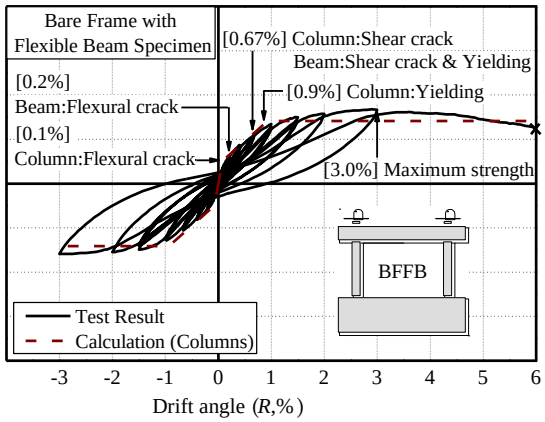

(b) BFFB specimen

Fig. 6 Lateral strength and drift angle relation of bare frame specimens

3.2 A simplified skeleton curve for URM infill

The simplified modeling method of the backbone curve for URM infill is discussed in more detail. The lateral load carried only by URM infills in IFRB and IFFB specimens are shown in Fig. 7 (Jin *et al*. 2016). As shown in the figure, the stiffness degradation was found before the lateral load reached its maximum value in both specimens. Then, the lateral load decreased after the maximum, and it remained almost constant in the larger drift angle. The backbone curve of URM infill surrounded by RC frame was therefore simplified, as shown in Fig. 8. Herein, characteristic points of cracking (R_{cr}, $V_{in,cr}$), maximum (R_{max}, $V_{in,\max}$), and residual strength (R_{res}, $V_{in,res}$) were adopted to represent the envelope, which will be explained in the next sub-section.

3.2.1 Cracking strength of URM infill

The cracking strength $V_{in,cr}$ of URM infill (shown 'A' in Fig. 8) is first discussed. In the previous study by Paulay and Priestley (1992), the cracking strength $V_{in,cr}$ of URM infill is shown to lie in the range of 50% to 70% of the maximum strength $V_{in,\max}$ of the infill which will be discussed later. On the other hand, the case where the cracking strength $V_{in,cr}$ exceeded 70% of the maximum strength $V_{in,\max}$ was observed in the authors' test results at around the drift angle of 0.1% which corresponded to the cracking point, as shown in Fig. 7. Therefore, the upper

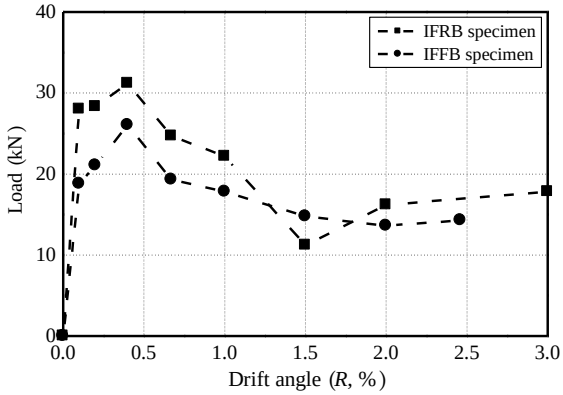

Fig. 7 Lateral load carried by URM infill from experimental result

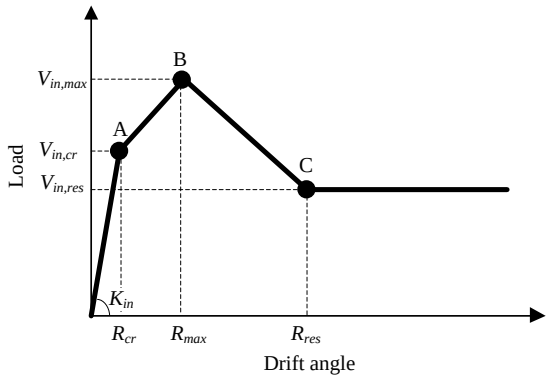

Fig. 8 Simplified envelope of URM infill

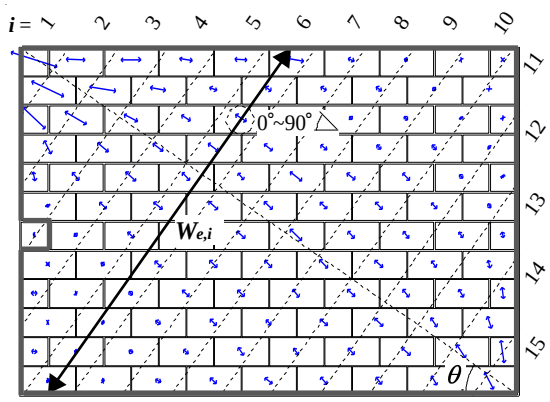

(a) IFRB specimen

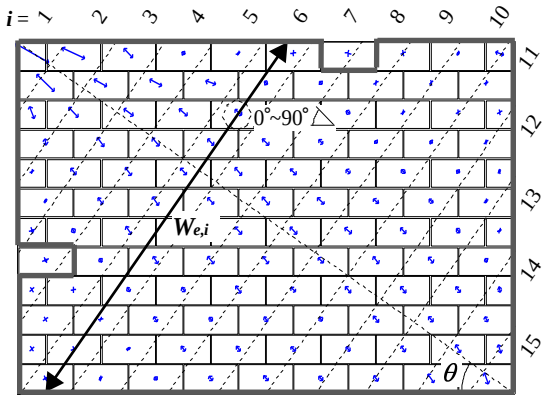

(b) IFFB specimen

Fig. 9 URM infill division and principal compressive strain distribution at 0.1% drift angle from experimental results

limit shown in the reference (Paulay and Priestley 1992), 70% of the maximum strength $V_{in,\max}$, was adopted for the cracking strength $V_{in,cr}$.

3.2.2 Drift angle at cracking strength of URM infill

The drift angle R_{cr} at cracking strength of URM infill is calculated from the ratio of the cracking strength $V_{in,cr}$ to the initial lateral stiffness K_{in} of the infill; that is, $R_{cr}= V_{in,cr}/K_{in}$. As shown in Eq. (7), the lateral stiffness converted from the axial stiffness of equivalent diagonal strut of URM infill was employed for K_{in}, which is the same method as ASCE41-06 (2006) and FEMA306 (1998). In this equation, the Young's modulus E_m of URM infill is obtained from the conventional 3-layered URM prism tests, and the diagonal strut angle θ is set to be the height-to-length angle of the infill for a simplified estimate.

$$K_{in} = E_m \cdot W_{eq} \cdot \cos^2\theta \cdot t / l_d \tag{7}$$

where E_m is the Young's modulus of URM infill, W_{eq} is the equivalent diagonal strut width, θ is the diagonal strut angle, t is the infill thickness, and l_d is the diagonal length of URM infill.

The equivalent diagonal strut width W_{eq} in Eq. (7) is then required to calculate K_{in}. Hence, the effective strut width $W_{e,i}$ and the principal compressive strain ε_i of the diagonal strut acting on the infill, which are necessary factors to estimate W_{eq}, will be reviewed from the previous experimental results (Jin *et al*. 2016), as below.

Effective diagonal strut width $W_{e,i}$

As stated above, the effective strut width $W_{e,i}$, a necessary parameter to estimate the equivalent diagonal strut width W_{eq}, is reviewed. As was done in the previous study (Jin *et al*. 2016), the URM infill was first divided into 15 sections (i=1 to 15) at equal intervals along the diagonal direction, as shown in Fig. 9, which was the smallest distance to include at least one compressive strain in each section. In this figure, the principal compressive strains of all URM units, obtained from 3-axis strain gauges at 0.1% drift angle, are shown together. Herein, only principal compressive strain angles between 0° and 90° were assumed to contribute to strut formation, and $W_{e,i}$ was defined as the length between the midpoints of outer faces of URM units having these angles in each section. As can be seen in Fig. 9, most principal compressive strains of URM units were found to have angles between 0° and 90°, as shown by the enclosed bold line. Therefore, in this study, $W_{e,i}$ was simply set to be the entire edge-to-edge distance of each section determined from the infill geometry, which was bounded by a column and a beam or by upper and lower beams. This assumption, open square symbols, is plotted together with the experimental results in Fig. 10, which shows good agreement. It should be noted that $W_{e,i}$ assumed in this study is slightly lower than the test results in some sections, because the assumed diagonal strut angle was slightly smaller than observed at the drift angle of 0.1% (IFRB≒39°, IFFB≒45°, Assumption≒35°).

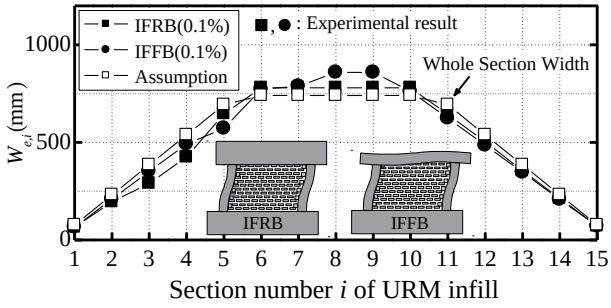

Fig. 10 Effective strut width $W_{e,i}$ (0.1%)

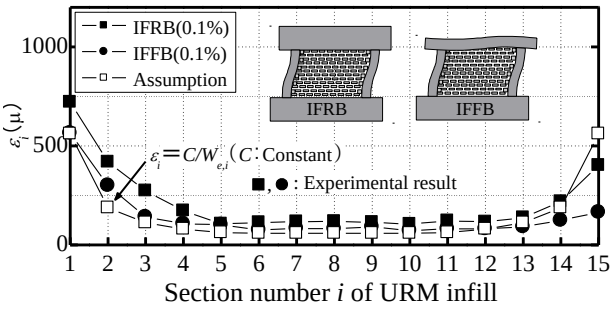

Fig. 11 Principal compressive strain ε_i (0.1%)

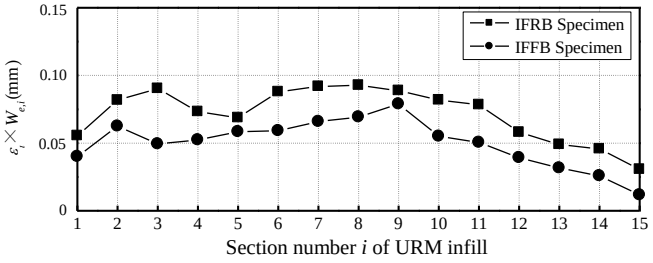

Fig. 12 ($\varepsilon_i \times W_{e,i}$) distribution from experimental results (0.1%)

Principal compressive strain ε_i

The principal compressive strain ε_i, which is another crucial parameter to estimate the equivalent diagonal strut width W_{eq}, is next reviewed. As was done in the previous study (Jin *et al*. 2016), ε_i is defined as the average value of principal compressive strains with angles between 0° and 90° in section *i*, which is shown in Fig. 11. As shown in the figure, the distribution of ε_i was found to have a shape roughly inversed to that of the effective strut width $W_{e,i}$ shown in Fig. 10. From this observation, the values of ε_i and $W_{e,i}$ ($\varepsilon_i \times W_{e,i}$) in 15 sections were investigated, as shown in Fig. 12, and these values were found to be roughly constant over all sections in both specimens. Therefore, ε_i was assumed to be inversely proportional to $W_{e,i}$; that is, $\varepsilon_i = C/W_{e,i}$, where C is a constant. It should be noted that the particular value of C is immaterial for calculating W_{eq}, which will be discussed later in Eqs. (8) and (9). The assumed theoretical distribution of ε_i, open square symbols, is plotted together with the experimental results in Fig. 11. In this figure, the average value of ε_1 and ε_{15} from the test results of IFRB specimen, as well as the average value of $W_{e,1}$ and $W_{e,15}$ assumed in the previous paragraph, was employed to determine the constant C, and their distribution also showed good agreement.

Equivalent diagonal strut width W_{eq}

The equivalent diagonal strut width W_{eq} is finally evaluated according to Eqs. (8) and (9), which assume that the same compression force P is applied to the original and equivalent strut sections, as shown in Fig. 13. In these equations, the effective diagonal strut width $W_{e,i}$ was obtained by the infill geometry, and the principal compressive strain ε_i was substituted for $C/W_{e,i}$, as explained earlier. W_{eq} was then calculated as 270mm from Eq. (9), which is about 25% of the diagonal length l_d of URM infill. The calculation result of $0.25l_d$ could almost approximate the overall experimental results of W_{eq} with a slightly conservative evaluation (Jin *et al*. 2016), as shown in Fig. 14, and was found to be consistent with the value proposed by Paulay and Priestley (1992). In addition, W_{eq} was also calculated to be about $0.25l_d$ in the URM infills with different aspect ratio γ_{in} (1.0 and 2.0), defined as l_{in} (infill length)/h_{in} (infill height), based on the same assumption and estimation method as done in the previous paragraphs; in other words, $\varepsilon_i = C/W_{e,i}$, and $W_{e,i}$ is the entire edge-to-edge distance of each section determined from the infill geometry.

$$W_{eq} = \sum_{i=1}^{n} (\varepsilon_i \times W_{e,i}) / \sum_{i=1}^{n} \varepsilon_i \tag{8}$$

$$W_{eq} = \sum_{i=1}^{n} (C / W_{e,i} \times W_{e,i}) / \sum_{i=1}^{n} (C / W_{e,i}) = n / \sum_{i=1}^{n} (1 / W_{e,i}) \tag{9}$$

where ε_i is the mean value of the principal compressive strain in section *i*, $W_{e,i}$ is the effective diagonal strut width in section *i*, and n is 15.

Because the aspect ratio γ_{in} of URM infill is generally between 1.0 and 2.0 in many buildings, γ_{in} was set to be their average value of 1.5 in the previous study (Jin *et al*. 2016), and a number of strain gauges were then used to precisely estimate the equivalent diagonal strut width W_{eq}. In some studies, γ_{in} has an effect on the variation of W_{eq}. In the studies by Stafford Smith (1969) and Hendry (1990), W_{eq} decreases as γ_{in} increases, and W_{eq} increases as γ_{in} decreases. However, in their studies, the fluctuation in W_{eq} is within about ±15%, when γ_{in} changes from 1.5 to 2.0 or from 1.5 to 1.0 (Chrysostomou and Asteris 2012), which is not a wide change. Additionally, W_{eq} proposed by Mainstone (1971), as well as Paulay and Priestley (1992), has an almost constant value with different aspect ratio γ_{in}. The relative stiffness between boundary RC frame and URM infill was also considered in those studies to estimate W_{eq} using a parameter of $\lambda_1 h_c$, where λ_1 is shown in Eq. (10) and h_c is the column height. According to these studies, W_{eq} decreases as the value of $\lambda_1 h$ increases, and W_{eq} increases as $\lambda_1 h_c$ decreases. On the other hand, in actual buildings with URM infill, the typical material characteristics and member size are not likely to widely vary; thus, the values of $\lambda_1 h_c$, which was about 3.2 in the previous study (Jin *et al*. 2016), would have a slight change. It should be noted that, in the study by Mainstone (1971), $\lambda_1 h_c$ merely has a slight effect on the change of W_{eq}, when $\lambda_1 h_c$ varies within this value. In addition, W_{eq} proposed in this study was found to be almost consistent with that of

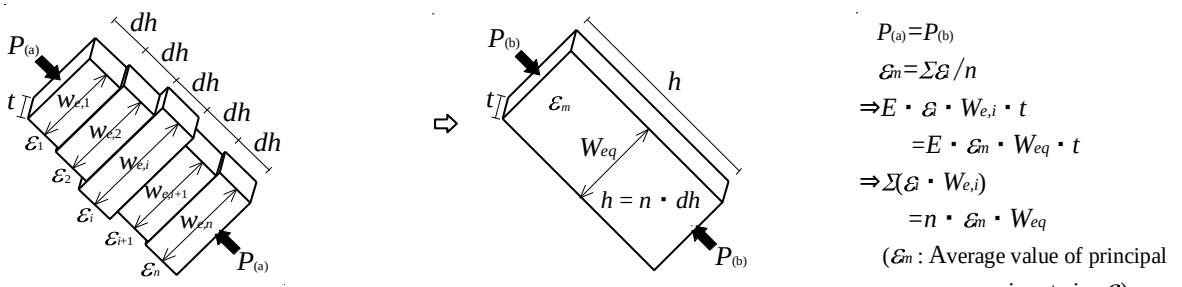

(a) Original strut (b) Equivalent Strut

Fig. 13 Equivalent diagonal strut width W_{eq}

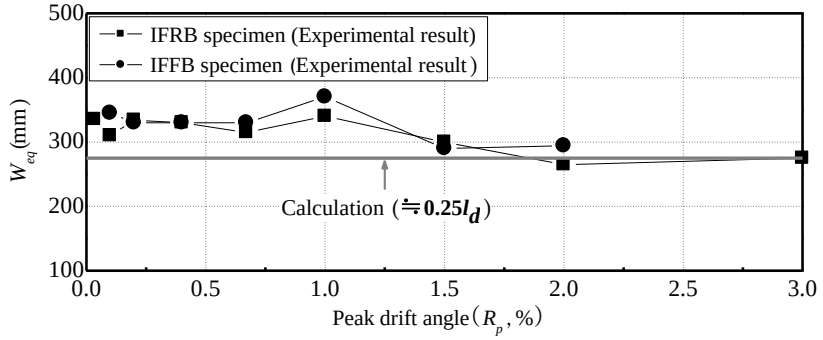

Fig. 14 W_{eq} between calculation and experimental results

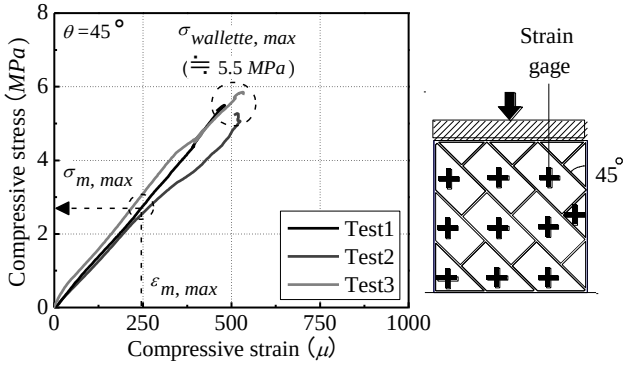

Fig. 15 URM wallettes and stress-strain relation

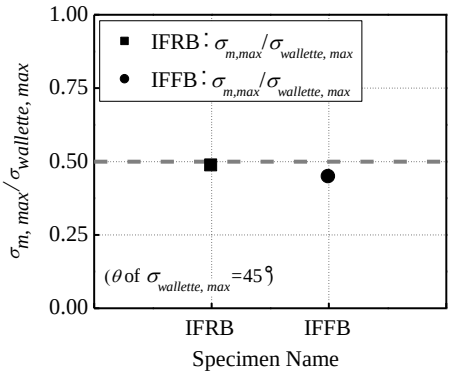

Fig. 16 $\sigma_{m,max}/\sigma_{wallette,max}$ (0.4%)

Hendry (1990), when the value of $\lambda_1 h_c$ was about 3.2 (Chrysostomou and Asteris 2012). For instance, in the case of a column section larger than 450mm by 450mm, a beam section larger than 300mm by 600mm, a slab thicker than 120mm, an infill height less than 2,700mm, an infill thickness approximately half of the column width, and the Young's modulus of the infill less than that of the previous study (Jin *et al*. 2016), the value of $\lambda_1 h$ would be smaller than 3.5. Therefore, W_{eq} proposed in this study would likely be almost a consistent or conservative value compared to that of Hendry (1990), and it is considered to be reasonably applicable to the URM infill with γ_{in} from around 1.0 to 2.0, where the value of $\lambda_1 h_c$ is less than 3.5.

$$\lambda_1 = \left[\frac{E_m \cdot t \cdot \sin 2\theta}{4E_{fe} \cdot I_c \cdot h_{in}}\right]^{1/4} \tag{10}$$

where E_m is the Young's modulus of URM infill, t is the infill thickness, θ is the angle of height to length of URM infill, E_{fe} is the Young's modulus of concrete, I_c is the moment of inertia of column, and h_{in} is the infill height.

The initial stiffness K_{in} is then calculated from Eq. (7), and the drift angle R_{cr} ($V_{in,cr}/K_{in}$) can be also obtained.

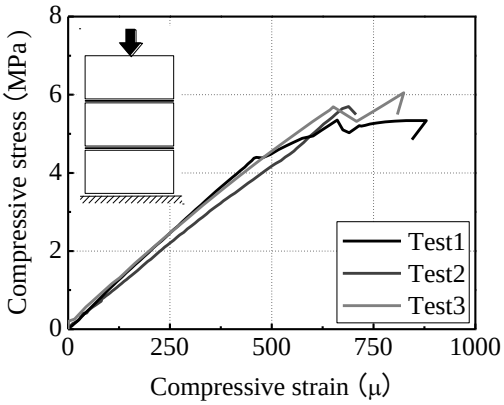

Fig. 17 Stress-strain relation of 3-layer stacked URM prism

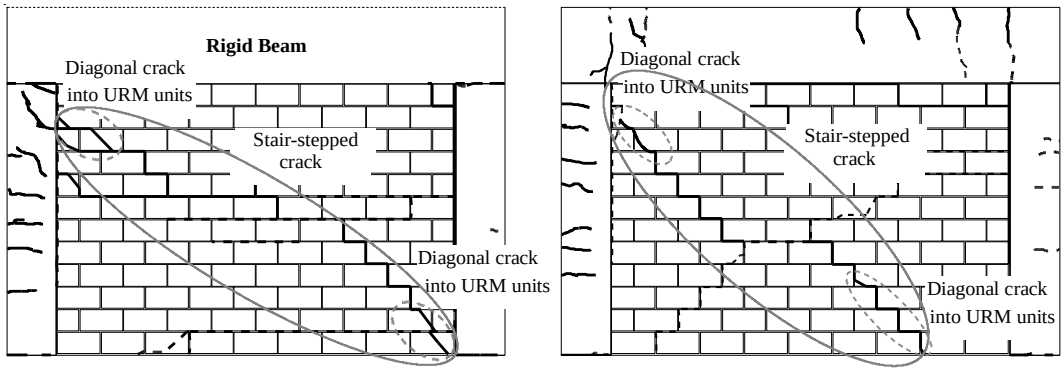

(a) IFRB specimen (b) IFFB specimen

Fig. 18 Damage state of URM infill at drift angle of 0.4% from experimental results

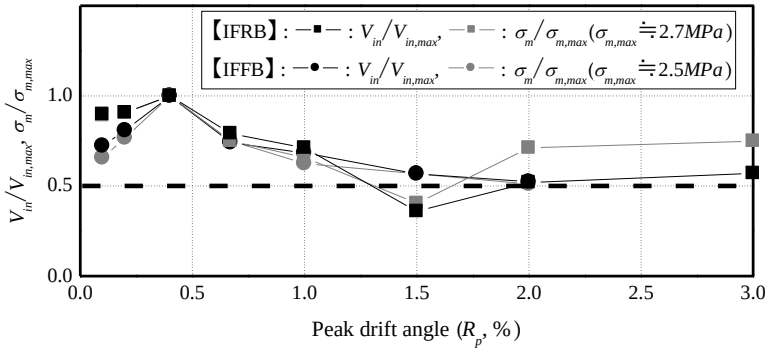

Fig. 19 Variation of V_{in} and σ_m of URM infill from experiment results

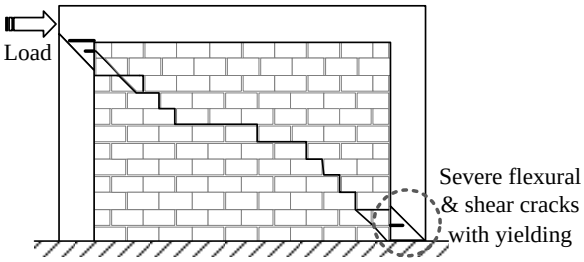

Fig. 20 Damage state of URM infill at residual strength

3.2.3 Maximum strength of URM infill

The maximum strength $V_{in,\max}$ of URM infill on the backbone curve shown in Fig. 8 (shown 'B') will be discussed. $V_{in,\max}$ of URM infill is evaluated according to Eq. (11). In this equation, the equivalent diagonal strut width W_{eq} is set to be $0.25l_d$, and the height-to-length angle of the infill is employed for the diagonal strut angle θ.

$$V_{in,\max} = W_{eq} \cdot \sigma_{m,\max} \cdot \cos\theta \cdot t \tag{11}$$

where W_{eq} is the equivalent diagonal strut width, $\sigma_{m,\max}$ is the maximum value of compressive stress σ_m acting on the equivalent diagonal strut at $V_{in,\max}$, θ is the diagonal strut angle, and t is the infill thickness.

The maximum value $\sigma_{m,\max}$ of the compressive stress σ_m is then required to calculate $V_{in,\max}$. In the previous study (Jin *et al*. 2016), to obtain the compressive stress σ_m acting on the equivalent diagonal strut, the average value ($\varepsilon_m=\Sigma\varepsilon_i/15$) of principal compressive strains ε_i in 15 sections of the infill was first calculated, and the corresponding σ_m was evaluated from the stress-strain relations of URM wallette tests (Fig. 15). It should be noted that, in the previous study, the wallette tests assuming three different strut angles (45°, 37.5° and 30°) were performed, and their test results were found almost similar, where the 45° URM wallette and its stress-strain relation is representatively shown in Fig. 15. In this study, the maximum value $\sigma_{m,\max}$ was accordingly evaluated from the compressive strength $\sigma_{wallette,\max}$ of the URM wallette, as shown in Fig. 16, and 45° wallette test was employed for $\sigma_{wallette,\max}$, since the diagonal strut angles in IFRB and IFFB specimens were closest to 45° at their maximum strength (IFRB:42°, IFFB:47°). As shown in Fig. 16, the ratio of the mean maximum value $\sigma_{m,\max}$ to the mean compressive strength $\sigma_{wallette,\max}$ in each test was found to be approximately 0.5 in both specimens; hence, $\sigma_{m,\max}$ acting on the equivalent diagonal strut was set to be 50% of $\sigma_{wallette,\max}$. When URM wallette tests are not available, however, $\sigma_{m,\max}$ might be substituted for half of the compressive strength of the 3-layered stacked URM prism, because their stress-strain relationships and maximum strength have been found to be almost similar, as shown in Figs. 15 and 17.

3.2.4 Drift angle at maximum strength of URM infill

The drift angle $R_{\max}$ at maximum strength of URM infill in RC boundary frame, with diagonal compressive strut, is not clear. However, the lateral strength of URM infill is considered to reach its maximum when the diagonal cracking is complete from corner to corner with the corner crushing.

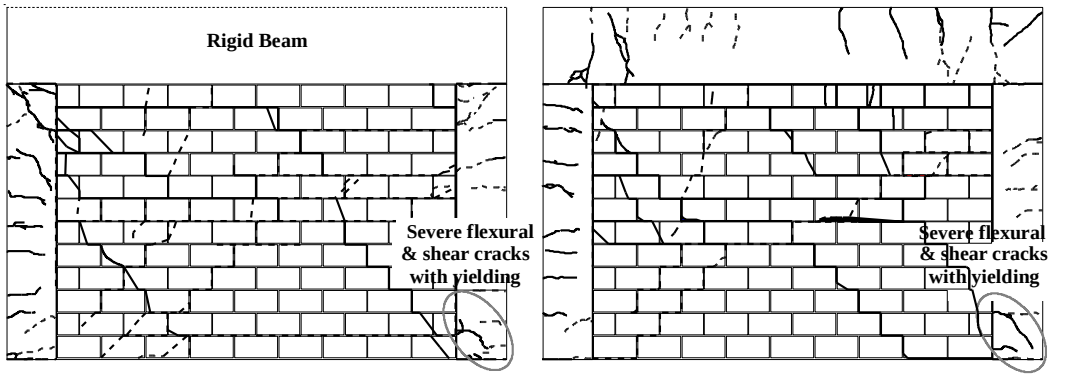

(a) IFRB specimen (b) IFFB specimen

Fig. 21 Damage state of URM infill at the drift angle of 1.0% from experimental results

Thus, the damage of URM infill was precisely observed from the previous experiments (Jin *et al*. 2016). As shown in Fig. 18, the stair-stepped crack fully developed in URM infill along with the diagonal strut, and diagonal cracks into URM units were also found on both ends of the strut at the drift angle of 0.4%. In the simplified evaluation, therefore, the lateral strength of URM infill was assumed to reach its maximum resulting in the full development of stair-stepped crack in the infill with corner crushing, and 0.4% drift angle was adopted for $R_{\max}$. According to FEMA306 (1998), the diagonal cracking in the infill begins and is complete from corner to corner with the onset of corner crushing between about 0.25% and 0.5% based on a number of experimental results, which reasonably agrees with $R_{\max}$ in this study.

3.2.5 Residual strength of URM infill

The residual strength $V_{in,res}$ of URM infill on the skeleton curve shown in Fig. 8 (shown 'C') is next discussed. The strength deterioration of URM infill began immediately after the maximum strength $V_{in,\max}$, and its residual shear resistance $V_{in,res}$ was almost 50% of $V_{in,\max}$ after the strength degradation, as shown in Fig. 19 (dashed line), where the lateral strength of the infill (V_{in}) is normalized by $V_{in,\max}$.

The half of $V_{in,\max}$ was therefore employed for the residual strength $V_{in,res}$ in the simplified evaluation. The variation of compressive stress σ_m acting on the equivalent diagonal strut, where σ_m is also normalized by $\sigma_{m,\max}$, is shown together in Fig. 19. As can be seen in the figure, the lateral resistance V_{in} was found mainly dependent on the compressive stress σ_m, so the reduction of V_{in} to 50% of $V_{in,\max}$ can be attributed to 50% decrease in σ_m.

3.2.6 Drift angle at residual strength of URM infill

The drift angle R_{res} at residual strength of URM infill is then discussed. The lateral strength of URM infill can be maintained after its maximum strength due to the confinement effect by boundary frames, and the compression column would be more contributable to the confinement of the infill than the tensile column (Fig. 20). Thus, R_{res} is assumed to be determined from the damage state of the compression column. In usual, with the yielding of a column, sever flexural and shear cracks tend to develop at the ends of the column, which is considered to degrade the confinement effect on the infill, and the stiffness of boundary frame would be almost constant without no increase. Therefore, it is assumed that the confinement effect on URM infill by RC boundary frame cannot be further expected after the yielding of the compression column, resulting in almost constant lateral resistance of the infill. It should be noted that those damage states were also observed at the drift angle of 1.0% in both specimens, as shown in Fig. 21, shortly after the compression column yielded. R_{res} is then calculated according to Eqs. (12) and (13), which are for the yielding deformation of RC column in bare frame. It should also be noted that the yielding deformation of the compression column with URM infill is likely to be larger than that without an infill, since the compressive axial force acting on the column section becomes larger due to the infill. On the other hand, these equations can conservatively estimate the yielding deformation of the compression column having URM infill, so it is employed for R_{res} in the simplified method.

$$R_{res} = 2M_{cu} / (h_c \cdot \alpha_y \cdot K_c) : \text{when } M_{cu} < M_{bu} \tag{12}$$

$$R_{res} = (M_{cu} + M_{bu}) / (h_c \cdot \alpha_y \cdot K_c) : \text{when } M_{cu} > M_{bu} \tag{13}$$

where M_{cu} is the ultimate bending moment of column, M_{bu} is the ultimate bending moment of beam, h_c is the column height, and $\alpha_y \cdot K_c$ is the secant stiffness of column (Eq. (4)).

In the next chapter, the simplified skeleton curve, proposed in this study, will be compared with the test results of IFRB and IFFB specimens (Jin *et al*. 2016), and it will be also compared with those estimation results by ASCE41-06 (2006). In addition to IFRB and IFFB specimens, more experimental results for URM-infilled RC frames are investigated, and the proposed backbone curves will be applied to them.

4. Skeleton curve evaluation result of URM-infilled RC frame

The skeleton curve evaluation results from the simplified method, for IFRB and IFFB specimens, are

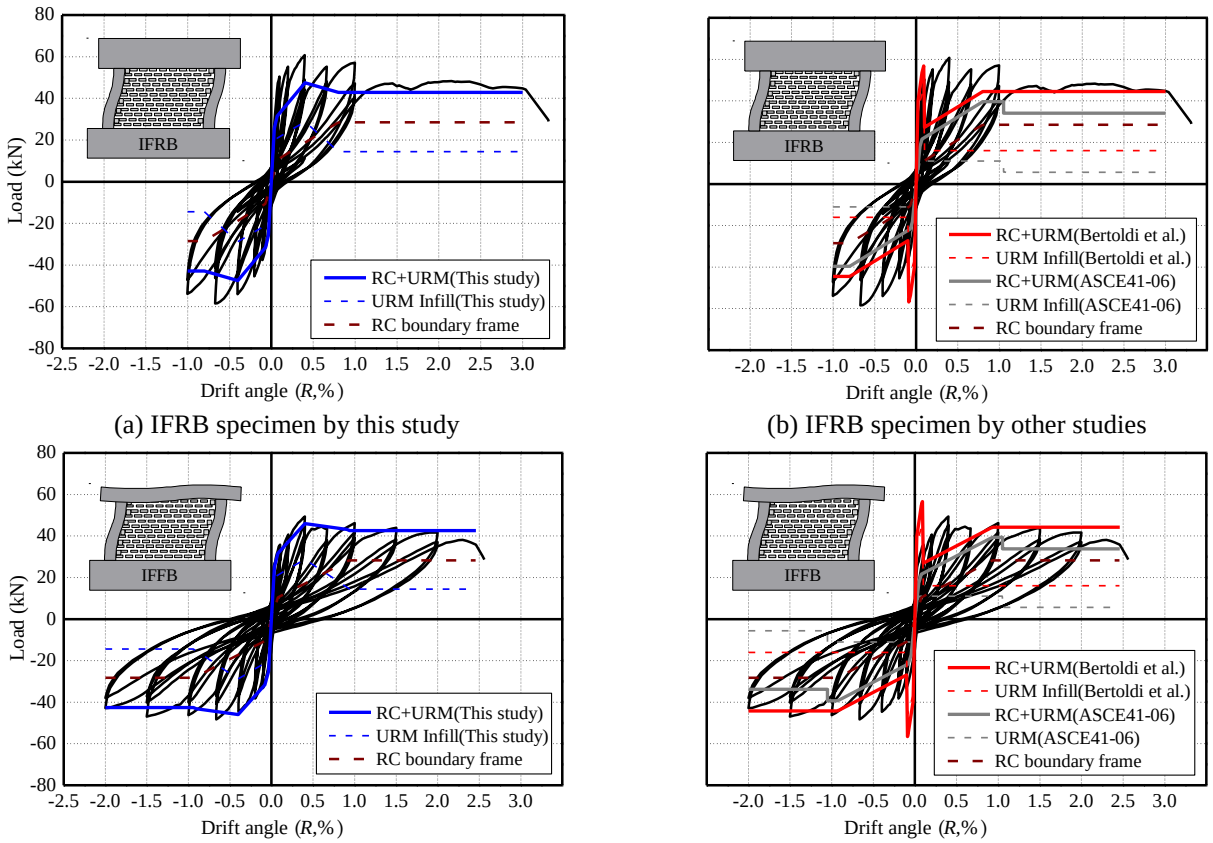

(a) IFRB specimen by this study

(b) IFRB specimen by other studies

(c) IFFB specimen by this study

(d) IFFB specimen by other studies

Fig. 22 Skeleton curve evaluation results of IFRB and IFFB specimens

demonstrated in Fig. 22. The backbone curves of URM infills, based on ASCE41-06 (2006) and Bertoldi *et al.* (1993), are also plotted in the figure, where the force-displacement envelope of RC boundary frame is identical in each specimen. In the backbone curve of URM infill based on ASCE41-06, the maximum strength V_{ine} was calculated from Eqs. (14) and (15), where v_{tL} was set to be its upper limit of 0.69MPa (100psi). P_D in Eq. (15) was assumed to be zero, since the dead load is likely to apply into RC boundary frame in this type of buildings. It should also be noted that the residual strength of URM infill was assumed to be half of V_{ine}. On the other hand, the skeleton curve by Bertoldi *et al.* (1993) was calculated from the diagonal compression strut action of the infill considering the relative stiffness between boundary columns and infills (Trapani *et al.* 2015).

$$V_{ine} = A_{ni} \cdot f_{vie} \tag{14}$$

$$f_{vie}(v_{me}) = 0.75 \cdot (0.75 v_{tL} + P_D / A_{ni}) / 1.5 \tag{15}$$

where A_{ni} is the infill section area, f_{vie} is the expected shear strength of the infill which shall not exceed the expected bed-joint shear strength v_{me}, v_{tL} is the lower-bound bed-joint shear strength which shall not exceed 0.69MPa (100psi), and P_D is the superimposed dead load at the top on the infill under consideration.

As shown in Fig. 22, the backbone curves for RC boundary frame and URM infill, as well as following overall envelopes, proposed in this study, reproduced reasonable correspondence with the test results (Fig. 4). The simplified skeleton curve for RC boundary frame was somewhat lower than the experimental result in IFRB specimen, since the tensile column in this specimen had acted as a short column from the test result in the early stages of loadings, as explained earlier (Jin *et al.* 2016). However, the overall envelop, which is the sum of RC boundary frame and URM infill, still showed a conservative evaluation having much better agreement than the calculation result using ASCE41-06. The load-deflection curves using ASCE41-06's method highly underestimated the test results, and those employing Bertoldi *et al.*'s method were likely to overestimate either the initial stiffness or the maximum strength. Also, both methods did not well reflect the seismic behavior after post-peak lateral strength, where they assumed sudden drop of the infill strength.

In addition to IFRB and IFFB specimens, more experimental results for URM-infilled RC frames conducted by other studies were investigated. The specimen details including member sizes and material characteristics are summarized in Table 1. These specimens are from one-third to half-scaled models, and the aspect ratio γ_{in} of the infill is in the range from 1.0 to 1.5. Also, the value of $\lambda_1 h_c$ was almost lesser than 3.5 in all specimens, which means the equivalent diagonal strut width $W_{eq}(0.25 l_d)$ proposed in this study would be appropriate to apply to all specimens. The skeleton curve evaluation results based on this study, as

Table 1 Member size, design detail, and material properties

	Specimen name	$F_{1,1,9}$ [*a]	Speci-men 4 [*b]	Speci-men 6 [*b]	Speci-men7 [*b]	IFOP [*c]
RC Boundary Frame	Column width (mm)	150	178	203	203	140
	Column depth (mm)	150	178	203	203	140
	Beam width (mm)	100	152	152	152	700
	Beam depth (mm)	200	229	229	229	550
	Concrete Comp. strength (MPa)	27.9	26.8	25.8	33.4	26.6
	Column main bar / Yielding strength (MPa)	8-ϕ6 348	8-D13 420	8-D16 413	8-D16 413	4-ϕ9 338
	Beam main bar / Yielding strength (MPa)	6-ϕ6 348	4-D16 413	4-D16 413	4-D16 413	12-D19 N.A
URM Infill	Infill height (mm)	860	1,422	1,422	1,422	1,000
	Infill length (mm)	860	2,057	2,057	2,057	1,460
	Infill width (mm)	90	92	92	92	44
	Stacked prism strength (MPa) [*d]	1.9	5.5	5.2	13.5	16.3
	Young's modulus (N/mm^2) [*e]	1,045	3,025	2,860	9,067	7,946

[*a] Experiment by Stylianidis (2012)
[*b] Experiment by Mehrabi *et al*. (1996)
[*c] Experiment by Maidiawati *et al*. (2012), Oo *et al*. (2012)
[*d] Compressive strength for gross section area.
[*e] Young's modulus was taken as 550 times the compressive strength, when it was not available

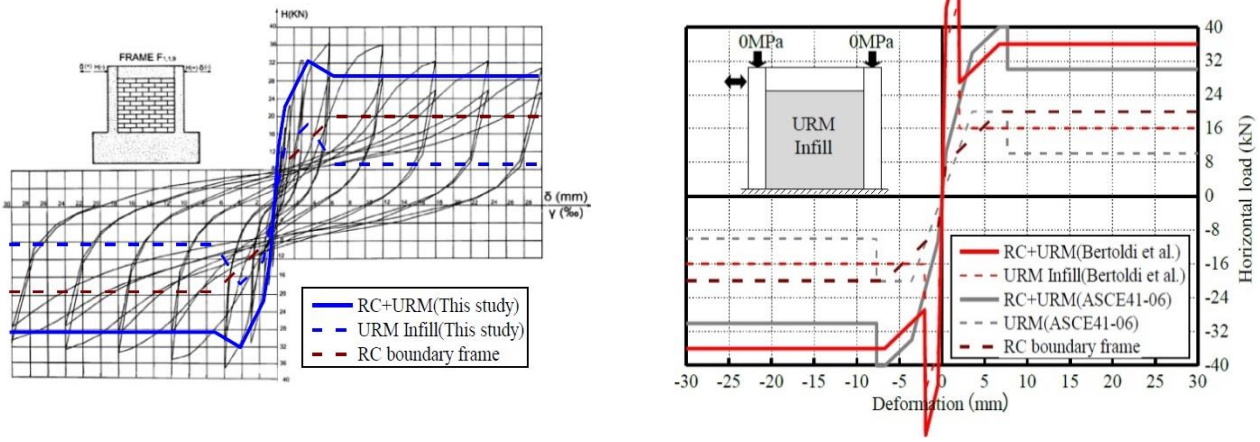

(a) Skeleton curve by this study (b) Skeleton by curve other studies

Fig. 23 Application example to experimental result of F1,1,9 (Stylianidis 2012)

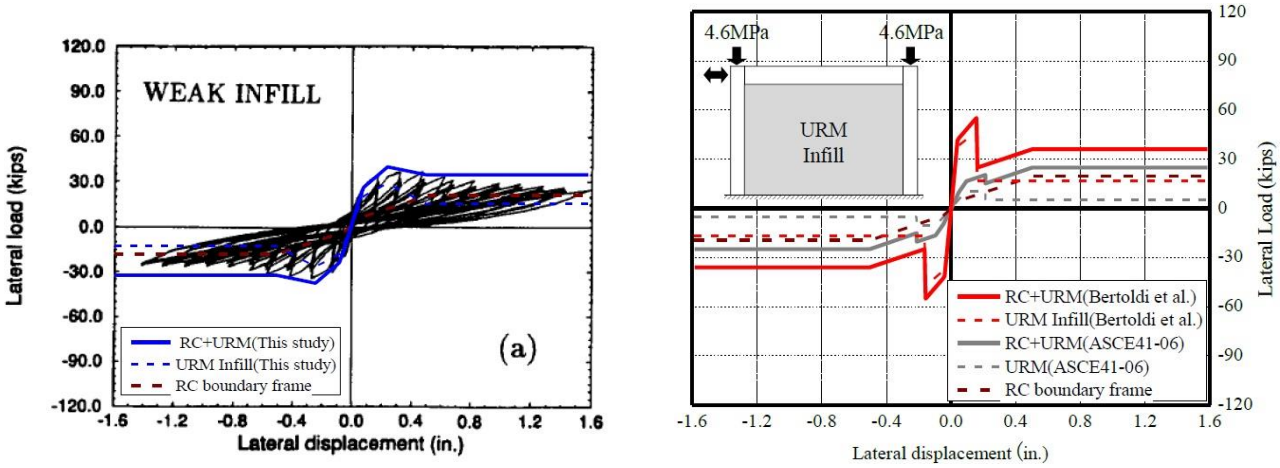

(a) Skeleton curve by this study (b) Skeleton by curve other studies

Fig. 24 Application example to experimental result of Specimen 4 (Mehrabi *et al*. 1996)

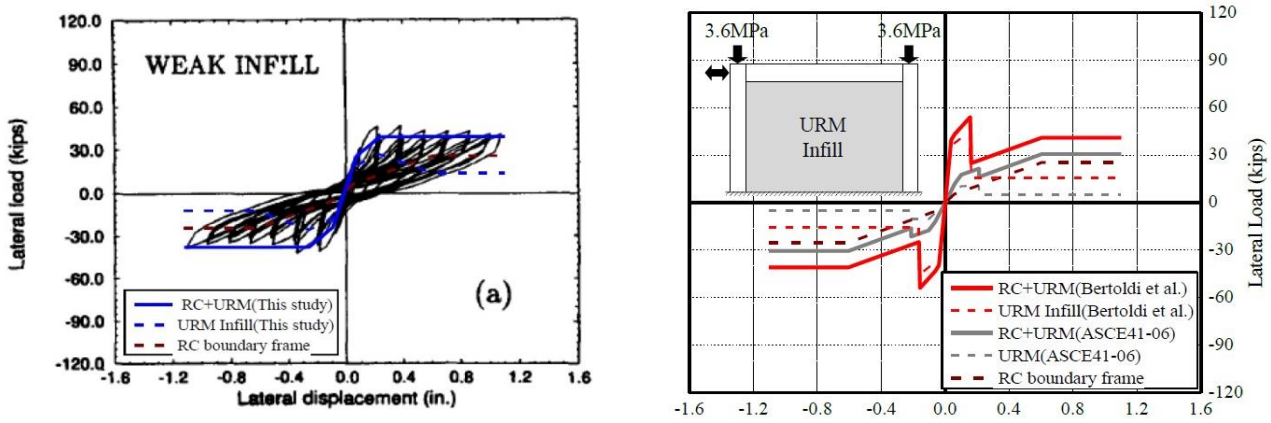

(a) Skeleton curve by this study (b) Skeleton by curve other studies

Fig. 25 Application example to experimental result of Specimen 6 (Mehrabi *et al*. 1996)

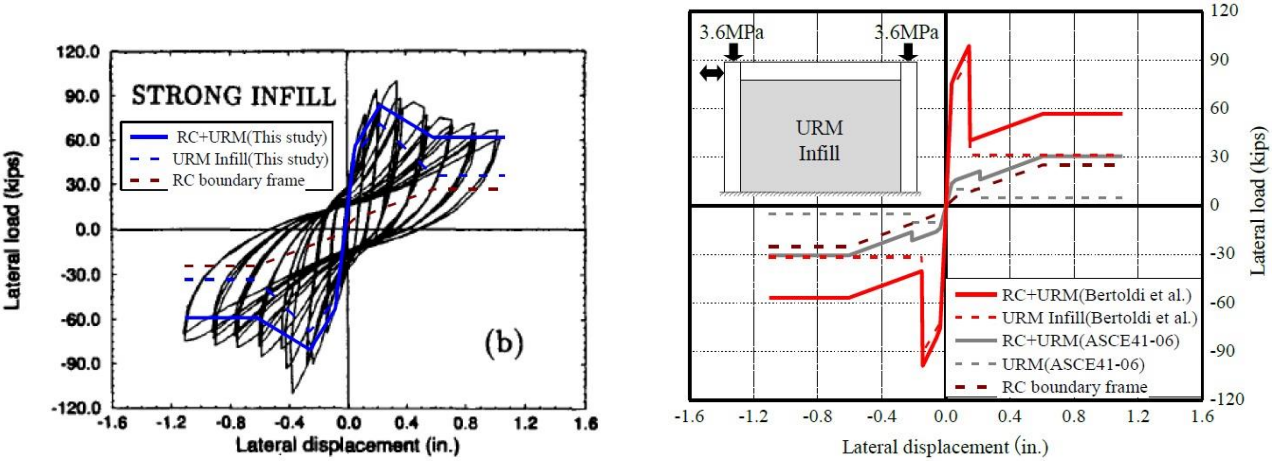

(a) Skeleton curve by this study (b) Skeleton by curve other studies

Fig. 26 Application example to experimental result of Specimen 7 (Mehrabi *et al*. 1996)

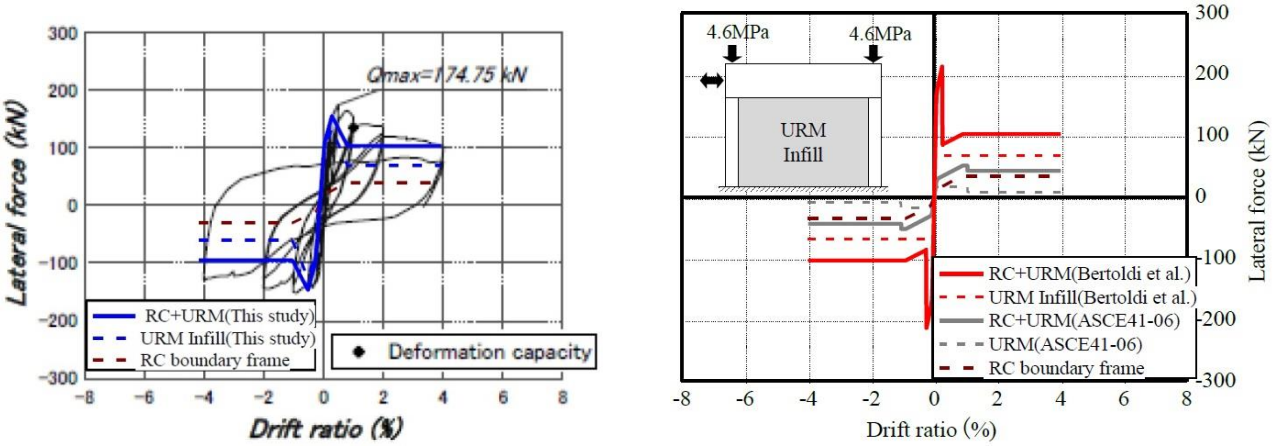

(a) Skeleton curve by this study (b) Skeleton by curve other studies

Fig. 27 Application example to experimental result of IFOP (Maidiawati *et al*., Oo *et al*. 2012)

well as by ASCE41-06 and Bertoldi *et al*., are compared with the experimental results in Figs. 23 through 27, where those of RC boundary frames were derived from Eqs. (1) through (6).

It should be noted that, for the relatively small-scaled specimens shown in Figs. 23 and 27, the ultimate bending moments of columns and beams (M_{cu}, M_{bu}) were calculated from the plane-section assumption, where the ultimate strain ε_{cu} at the concrete compression fiber was set to be 0.003.

As shown in Figs. 23 through 27, the simplified estimation results, proposed in this study, were found to almost approximate the overall response through all experimental results collected in this paper; also they showedmuch better agreement with those test results than the cases employing the infill envelopes from ASCE41-06 and Bertoldi *et al*. The estimation results using ASCE41-06 showed conservative evaluates in most experimental results, but they did not faithfully reflect the different strength of URM units, as shown in those figures. The results using Bertoldi *et al*.'s method tended to overestimate the initial stiffness and maximum strength, as was found in Fig. 22. Especially in both methods, the seismic behavior after the post-peak lateral strength was not well predicted due to abrupt decrease of the infill strength.

In this paper, a simplified procedure for the skeleton curve estimation of URM infilled-RC frames was proposed based on the previous experimental results having a number of detailed strain data, and the evaluation results were compared with existing literatures. The method is useful in preliminary design process by practical engineers to understand the general behavior expected by URM infills. The proposed method provided good estimation for the overall behavior of infilled-RC frames based on the interaction effect between boundary frames and the infills. Also, the seismic behavior after post-peak lateral strength was reasonably reproduced using the proposed model, which was not well predicted by previous models.

5. Conclusions

A simplified evaluation method of the skeleton curve for URM-infilled RC frames was proposed in a practical form, based on the previous studies. The major findings can be summarized as follows.

• The skeleton curve of RC boundary frame was modeled by a tri-linear envelope, similarly to that of RC bare frame, for simplified and conservative modeling. In contrast, that of URM infill was modeled by representative characteristic points of cracking, maximum, and residual strength, based on the previous study by authors (Jin *et al*. 2016) having detailed strain data of the infill.

• The cracking strength of URM infill was set to be 70% of its maximum strength. The equivalent diagonal strut width of URM infill was proposed as 25% of the diagonal length of the infill. This value was found to be consistent with the result of Paulay and Priestley (1992), and it also agreed with that of Henry (1990), when considering the relative stiffness between the infill and boundary frame of the specimens in the previous study by authors.

• The maximum value of compressive stress acting on the equivalent diagonal strut was set to be 50% of the URM wallette test carried out in the previous study by authors. When the URM wallette tests are not available, however, half of the compressive strength of stacked URM prism might be also employed.

• The lateral strength of URM infill was assumed to reach its maximum value resulting from the full development of stair-stepped crack with corner crushing, and the drift angle at maximum strength was set to be 0.4% from the previous experiment by authors. These damage state and drift angle of URM infill were found to reasonably agree with FEMA306 (1998).

• The residual strength of URM infill was set to be 50% of its maximum strength. The confinement effect on URM infill by RC boundary frame was assumed not to be further expected after the yielding of the compression column, resulting in almost constant lateral resistance of the infill. The drift angle at residual strength of URM infill was then proposed as the yielding drift of the compression column.

• The simplified estimation results proposed in this study could almost approximate the experimental results collected in this paper, and they also showed much better agreement with those test results than the cases employing the infill envelopes from ASCE41-06 (2006) and Bertoldi *et al*. (1993).

References

ACI Committee 318 (2011), *Building Code Requirements for Structural Concrete (ACI 318-11) and Commentary*, American Concrete Institute, Farmington Hills, MI.

AIJ (2010), *AIJ Standard for Structural Calculation of Reinforced Concrete Structures*, Architectural Institute of Japan, Tokyo.

Al-Chaar, G. (2002), "Evaluating strength and stiffness of unreinforced masonry infill structures (No. ERDC/CERL-TR-02-1)", Engineer Research and Development Center, U.S. Army Corps of Engineers.

ASCE/SEI 41-06 (2006), *Seismic Rehabilitation of Existing Buildings*, American Society of Civil Engineers, New York.

Bertoldi, S.H., Decanini, L.D. and Gavarini, C. (1993), "Telai tamponati soggetti ad azioni sismiche un modello semplificato: Confronto sperimentale e numerico (Infilled frames subjected to seismic actions a simplified model: Experimental and numerical comparison)", *Atti del 6 Convegno Nazionale ANIDIS* (*Proceedings of the 6th national conference on seismic engineering ANIDIS*), 815-824, Perugia.

Caliò, I. and Pantò, B. (2014), "A macro-element modelling approach of Infilled Frame Structures", *Comput. Struct.*, **143**, 91-107.

Chrysostomou, C.Z. and Asteris, P.S. (2012), "On the in-plane properties and capacities of infilled frames", *Eng. Struct.*, **41**, 385-402.

FEMA 306 (1998), *Evaluation of Earthquake Damaged Concrete and Masonry Wall Buildings*, Applied Technology Council (ATC-43 Project), Washington D.C.

FEMA 356 (2000), *Prestandard and Commentary for the Seismic Rehabilitation of Buildings*, Washington D.C.

Fiorato, A.E., Sozen, M.A. and Gamble, W.L. (1970), "An investigation of the interaction of reinforced concrete frames with masonry filler walls", Rep. UILU-ENG 70-100, Univ. of Illinois, Urbana-Champaign, Ill.

Fiore, A., Netti, A. and Monaco, P. (2012), "The influence of masonry infill on the seismic behavior of RC frame buildings", *Eng. Struct*, **44**, 133-145.

Hendry, A.W. (1990), *Structural Masonry*, Macmillan, London, England.

Hetenyi, M. (1946), *Beams on Elastic Foundation*, University of Michigan Press, Ann Arbor.

Holmes, M. (1961), "Steel frames with brickwork and concrete infilling", *Proc. Instn. Civ. Engrs*, **19**(4), 473-478.

Jin, K., Choi, H. and Nakano, Y. (2016), "Experimental study on lateral strength evaluation of unreinforced masonry-infilled RC

frame", *Earthq. Spectra*, **32**(3), 1725-1747.
KMCT (2002), *A Study on the Seismic Evaluation and Retrofitting Methods for Low-Rise RC Buildings in Korea*, Korean Ministry of Construction and Transportation, Seoul.
Maidiawati, O.T. and Sanada, Y. (2012), "Static loading test of R/C frames with brick masonry infill with/without plaster (Part II: Test results and seismic performance evaluation)", *Summaries of Technical Papers of Annual Meeting*, Architectural Institute of Japan, **C-2 Structures IV**, 1055-1056.
Mainstone, R.J. (1974), "On the stiffness and strength of infilled frames", *Proc. Supplement, Trans. of Inst. of Civil Eng. State Univ. of New York*.
Mehrabi, A.B., Shing, P.B., Schuller, M.P. and Noland J.L. (1996), "Experimental evaluation of masonry-infilled RC frames", *J. Struct. Eng.*, **122**(3), 228-237.
Oo, T., Maidiawati and Sanada Y. (2012), "Static loading test of R/C frames with brick masonry infill with/without plaster (Part I: Test specimens and experimental methods)", *Summaries of Technical Papers of Annual Meeting*, Architectural Institute of Japan, **C-2 Structures IV**, 1053-1054.
Öztürkoğlu, O., Ucar, T. and Yesilce, Y. (2017), "Effect of masonry infill walls with openings on nonlinear response of reinforced concrete frames", *Earthq. Struct.*, **12**(3), 333-347.
Panagiotakos, T.B. and Fardis, M.N. (1996), "Seismic response of infilled RC frames structures", *Proceedings of 11th World Conference on Earthquake Engineering*, Acapulco.
Paulay, T. and Priestley, M.J.N. (1992), *Seismic Design of Reinforced Concrete and Masonry Buildings*, John Wiley & Sons, INC.
Shing, P.B. and Stavridis, A. (2014), "Analysis of seismic response of masonry-infilled RC frames through collapse", *ACI Struct. J.*, Special Publication, **297**, 1-20.
Stafford Smith, B. and Carter, C. (1969), "A method of analysis for infill frames", *Proc., Instn. of Civ. Engrs.*, **44**, 31-48.
Stavridis, A. and Shing, B. (2012), "Simplified modeling of masonry-infilled RC frames subjected to seismic loads", *Proceedings of 15th World Conference on Earthquake Engineering*, Lisbon, Sep.
Stylianidis, K.C. (2012), "Experimental investigation of masonry infilled R/C frames", *Open Construct. Build. Tech. J.*, **6**, 194-212.
Sugano, S. (1970), "Experimental study on hysteretic characteristics of reinforced concrete members", Ph.D. Dissertation, The University of Tokyo, Tokyo.
Trapani, F.D., Macaluso, G., Cavaleri, L. and Papia, M. (2015), "Masonry infills and RC frames interaction: Literature overview and state of the art of macromodeling approach", *Eur. J. Environ. Civil Eng.*, **19**(9), 1059-1095.

CC